Vortex Mediated Fabrication of 2D Antimonene Sheets From Antimony Powder

Fayed Abdullah Alrashaidi,[a,b] Soraya Rahpeima,[a,c] Xuan Luo,[a] Kasturi Vimalanathan,[a] Abdulrahman S. Alotabi, [a,d] Thaar Alharbi, [e] Xianjue Chen, [f] Dechao Chen, [g] Youhong Tang,[a] Christopher Gibson, [a,h] Nadim Darwish, [c] Qin Li, [g] and Colin L. Raston [a*]

a. Flinders Institute for Nanoscale Science and Technology, College of Science and Engineering, Flinders University, Adelaide, SA 5042, Australia

b. Department of Chemistry, College of Science, Jouf University, Sakaka 72388, Saudi Arabia

c. School of Molecular and Life Sciences, Curtin Institute for Functional Molecule and Interfaces, Curtin University, Bentley, Western Australia 6102, Australia

d. Department of Physics, Faculty of Science and Arts in Baljurashi, Albaha University, Baljurashi 65655, Saudi Arabia

e. Physics Department, Faculty of Science, Taibah University, Almadinah, Almunawarrah 42353, Saudi Arabia

f. School of Environmental and Life Sciences, The University of Newcastle, Callaghan, New South Wales 2308, Australia

g. Queensland Micro- and Nanotechnology Centre, Griffith University, Brisbane, QLD 4111, Australia

h. Flinders Microscopy and Microanalysis, College of Science and Engineering, Flinders University, Adelaide, SA 5042, Australia

Address correspondence to colin.raston@flinders.edu.au

Author Contributions

F.A.J.A. carried out the synthesis, and SEM, XRD, XPS, and TGA-DSC studies, and wrote the draft of manuscript, S.R. and N. D. carried out C-AFM studies, D.C. and Q.L. carried out PL studies, T.A., K.V., C.G. and X.L. carried out Raman and AFM studies, X.C carried out TEM studies, A.A. carried out the XPS data-fitting, and C.L.R. coordinated the research and finalising the manuscript. All authors contributed to editing the manuscript.

List of contents

Materials and characterization

Antimony powder, 100-mesh, 99.5 % purity, was purchased from Sigma Aldrich. 2-Propanol (isopropanol) (IPA) was purchased from Chem supply, and N-N Dimethylformamide (DMF) anhydride 99.8% was purchased from Sigma Aldrich.

Scanning Electron Microscopy (SEM)

Scanning electron microscopy (SEM) images for determining the morphology of the samples were obtained using a FEI Inspect F50 SEM.

Raman Spectroscopy

Raman spectroscopic studies used a WITec alpha300R confocal Raman microscope at an excitation laser wavelength of 532 nm with a 100X objective (numerical aperture 0.9). The grating used was 600 grooves/mm which gives a spectral resolution of approximately 3 to 4 wavenumbers.

X-ray Diffraction (XRD)

XRD (Bruker D8 ADVANCE ECO, Bragg-Brentano geometry with a cobalt X-ray source, λ = 1.79 Å) was utilized for examining the crystal structure of Sb sheets. The data analysis for XRD used the ICDD PDF-2 Database, DIFFRAC. EVA Software was used for phase identification along with Top as the software package for crystal structure determination and quantitative phase analysis.

Atomic Force Microscopy (AFM)

AFM images were acquired using a Bruker Multimode 9 AFM with a Nanoscope V controller using tapping mode in air, with all parameters including set-point, scan rate and feedback gains adjusted to optimize image quality. The imaging resolution was set to 512 points/line. The AFM probes used were Mikromasch HQ: NSC15 Si probes with a nominal spring constant of 40 N/m and a nominal tip diameter of 16 nm. The scanner was calibrated in x, y and z directions using silicon calibration grids (Bruker model number VGRP: 10 μm pitch, 180 nm depth). All analysis of AFM images, including flattening and dimensional analysis, was performed using Nanoscope analysis software version 1.4.

Transmission Electron Microscopy (TEM)

Drop casting dispersions of antimonene onto a holey carbon-coated Cu grid was used to make the specimens for TEM, which were then dried in air. A JEOL JEM-F200 Multi-Purpose FEG-S/TEM with an operating voltage of 200 kV was employed for TEM/STEM analysis. The TEM and elemental mapping images were processed using Image J and Pathfinder.

Conductive Atomic Force Microscopy (C-AFM)

Current−voltage measurements were conducted using a Bruker Dimension AFM with an Icon head and a PeakForce tunneling AFM (PF-TUNA™) module. Measurements were carried out in air at room temperature using a solid conductive platinum tip (RMN-25PT300B) with a nominal spring constant of 18 N/m and nominal resonance frequency of 20 kHz. The imaging resolution was set to 256 points/line and scan rate of 1.00 Hz. Current detector sensitivity was adjusted to 100 nA/V.

UV-vis absorption and fluorescence spectroscopy:

The UV-vis absorption and fluorescence excitation and emission were measured with a Horiba Duetta. A Tauc Plot was derived from UV-vis absorption spectrum by applying the Tauc equation:

$(ahv)^2 = C(hv - E_g)$,

where a is absorption, h Planck constant, ν wavelength, C extinction coefficient, and E_g the bandgap

X-ray Photoelectron Spectroscopy (XPS)

Surface were studied using X-ray photoelectron spectroscopy (XPS). For X-ray irradiation, a UHV instrument with an Phoibos 100 hemispherical analyser (SPECS) and a base pressure of 3x 10-9 mbar was applied. A non-monochromatic X-ray source with a Mg anode (12 kV-200 W, Kα line with an excitation energy of 1253.6 eV) was utilized.

Scherrer equation for bulk Sb and 2D Sb thin sheets:

Where: the average crystalline domain size in Å is (τ)

The diffraction angle (θ)

The full width at half maximum (B), and the wavelength (λ) of the X-ray source: hence,

Sb Bulk $$\tau = \frac{0.9x0.179}{0.141\cos 33.51} = 71.4\ nm = \ 714\ \text{Å}$$

2D Sb sheets $$\tau = \frac{0.9x0.179}{0.209\cos 33.60} = 48.1\ nm \ = \ 481\ \text{Å}$$

We calculated the crystallite size for the 2D Sb sheets based on the Scherrer equation, which is smaller compared to bulk Sb. This illustrates the effectiveness of the rapid localized heating and melting of the as received Sb micron sized particles subjected to ST flow, with then rapid cooling and crystallization. The rapid cooling limits the time for crystal growth, which results in smaller crystallites in 2D Sb sheets.[1,2]

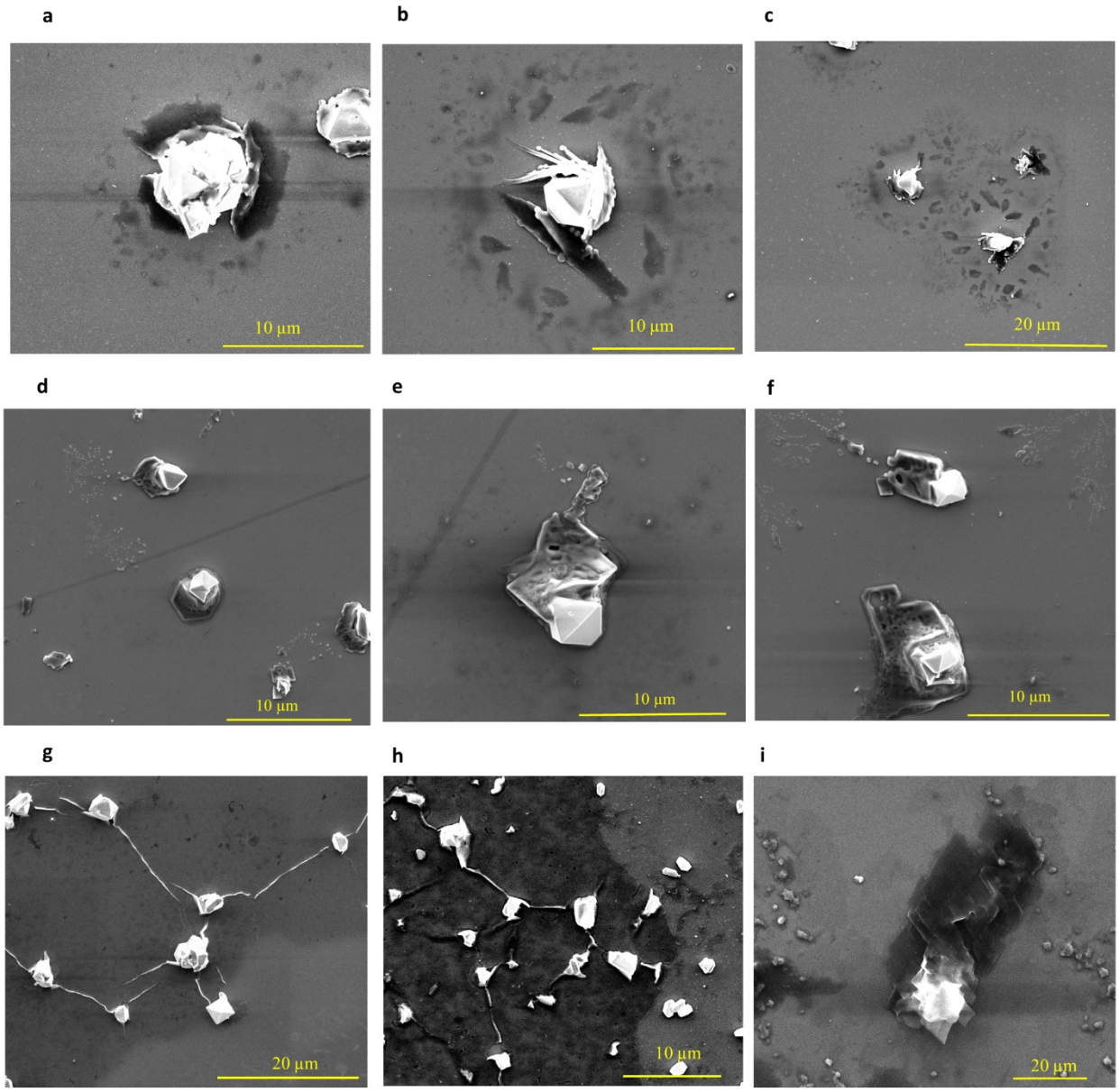

Figure S1. SEM images of primarily processed Sb (0.25 mg.mL^{-1}) in confined mode- VFD , (a-c) Sb dispersed in H_2O for 48 hours and processed in VFD for 30 seconds in air atmosphere, (d-f) Sb dispersed 1:1 mixture H_2O and IPA for 48 hours and processed in VFD for 1 min in air atmosphere, and (g-h) Sb dispersed 1:1 mixture of IPA and DMF for 48 hours and processed in VFD in air atmosphere for 2 mins. (i) Sb dispersed 1:1 mixture of IPA and DMF and processed in VFD in N_2 atmosphere for 2 mins.

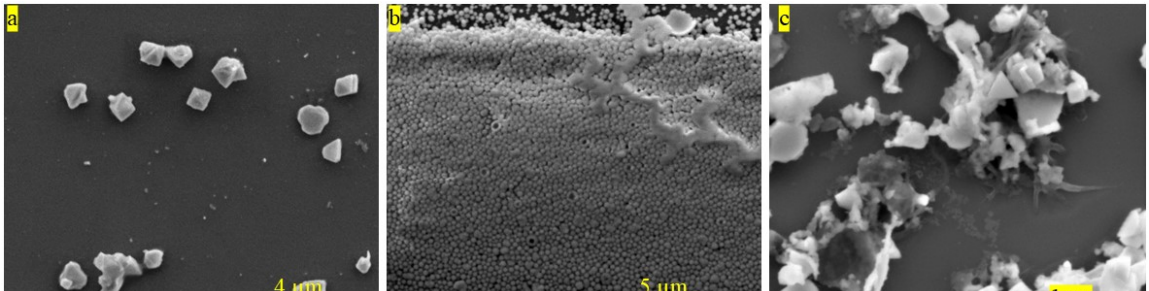

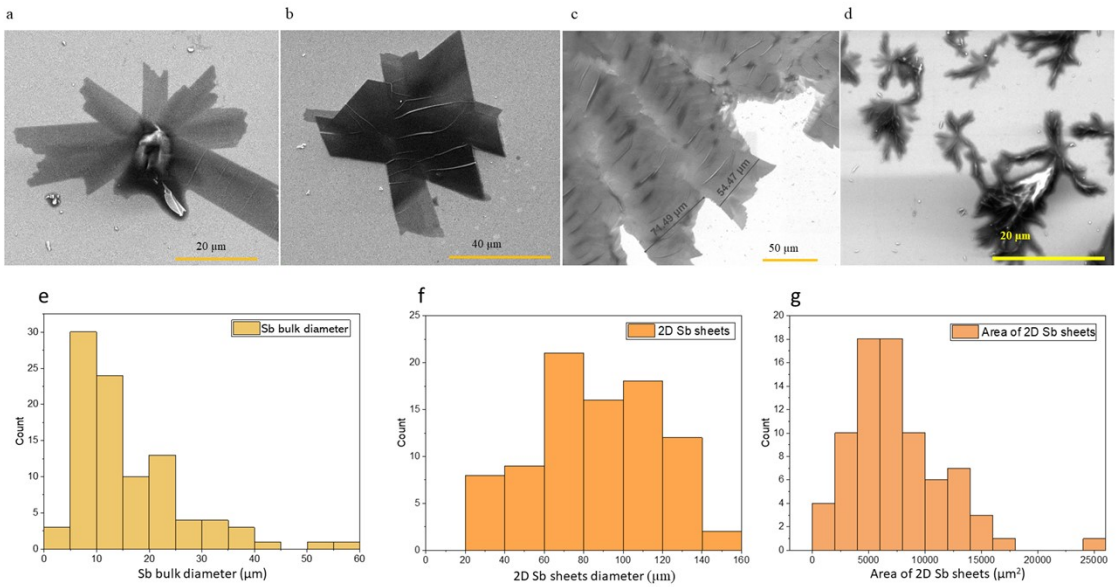

Figure S3. SEM images of VFD processed Sb in IPA and DMF, ratio 1:1 in different concentration, N_2 atmosphere, 45° tilt angle at room temperature. (a) Concentration 0.1 mg.mL^{-1} in 20 mm OD VFD tube in confined mode at 4.5k rpm. (b) Concentration 1 mg.mL^{-1} in 20 mm OD VFD in confined mode at 4.5k rpm. (c) Concentration 3 mg.mL^{-1} in 20 mm OD VFD in confined mode at 4.5k rpm. (d) Concentration 0.25 mg.mL^{-1} in 20 mm OD VFD tube at 4.5k rpm, - 45° tilt angle at room temperature in continuous flow with flow rate of 0.5 mL.min^{-1} affording rods. Particle size distribution for bulk Sb after mortar and pestle processing, (e), and for 2D antimonene after VFD processing, (f). (g) Area distribution of antimonene sheets.

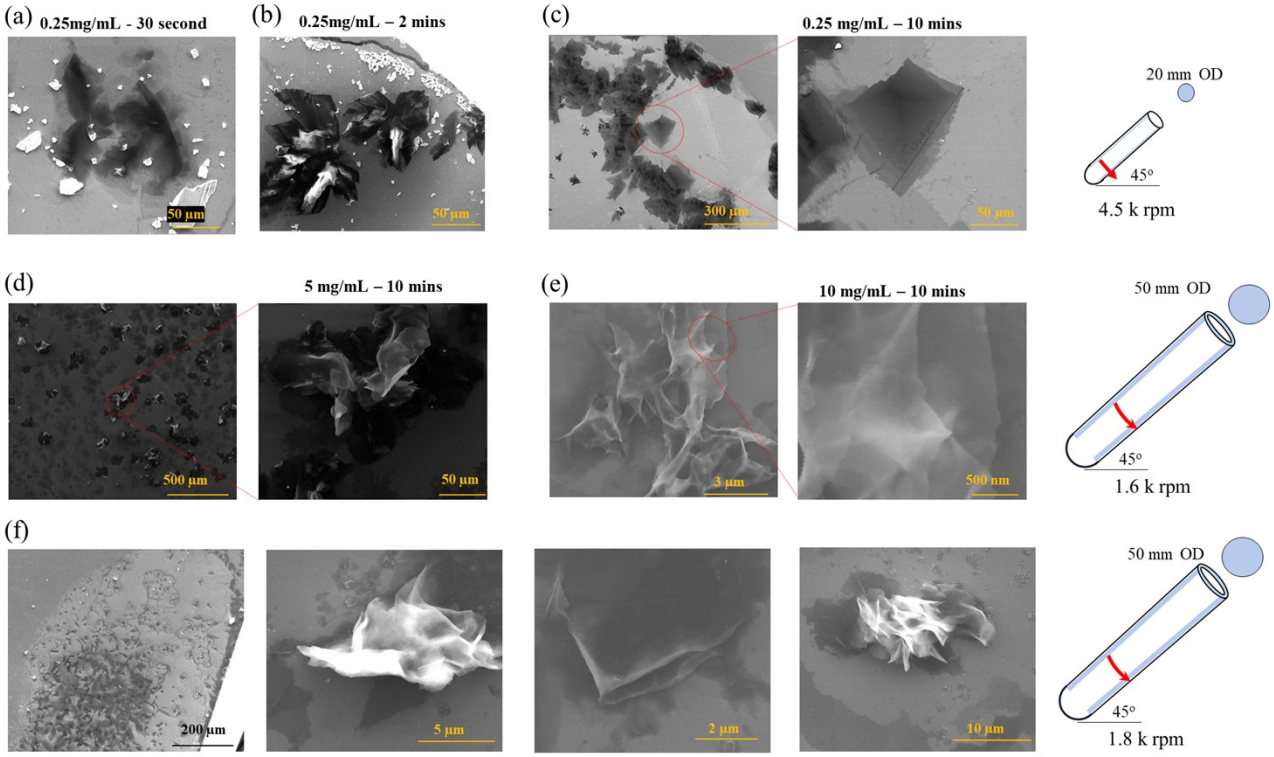

Figure S4. SEM images of VFD processed (confined mode) Sb in IPA and DMF (1:1), N_2 atmosphere, 45° tilt angle at room temperature. (a) Concentration 0.25 mg.mL^{-1} after 30 s in 20 mm OD VFD tube rotating at 4.5k rpm. (b) Concentration 0.25 mg.mL^{-1} in 2 min in a 20 mm OD VFD tube rotating at 4.5k rpm. (c) Concentration 0.25 mg.mL^{-1} in 10 min in 50 mm OD VFD tube at 1.6k rpm. (d) Concentration 5 mg.mL^{-1} in 10 min in a 50 mm OD VFD tube at 1.6k rpm. (e) Concentration 10 mg.mL^{-1} in 10 min in a 50 mm OD VFD tube rotating at 1.6k rpm. (f) Concentration 10 mg.mL^{-1} in 10 min in a 50 mm OD VFD tube rotating at 1.8k rpm in L-VFD.

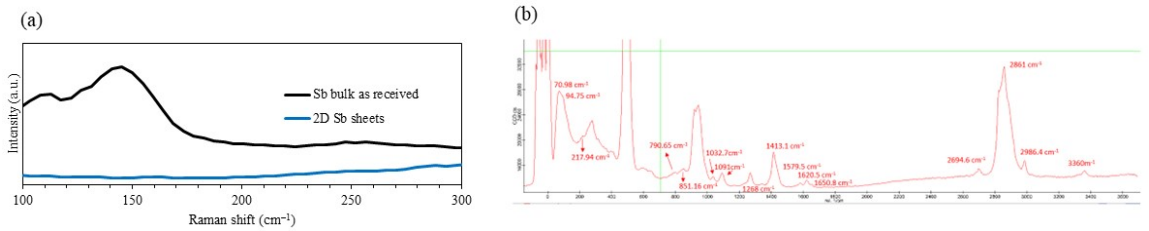

Figure S5. (a) Raman spectra of Sb as received and antimonene sheets fabricated in VFD using the optimised conditions, Fig. **1.** (b) . Raman spectra of thick antimonene sheets show 2D peak at 2694 cm^{-1} and C-H_3 at 2861 cm^{-1}.

The utility of Raman spectroscopy appears to be limited for 2D antimonene thin sheets.[3,4] The thin sheets of antimonene have a weak Raman signal and to our knowledge, there is no report for single layer antimonene. Indeed, previously, this unexpected relationship between Raman intensity and thickness of antimonene has been reported in micromechanically exfoliated Sb powder, there being no Raman signal for thicknesses less than ≈100 nm.[5] Even after using many laser excitation wavelengths and increasing the acquisition period (λ = 785, 633, 532, 473, 457, and 405 nm), no Raman signal was detected.[3] This result is consistent with the thickness of 2D antimonene determined using AFM.

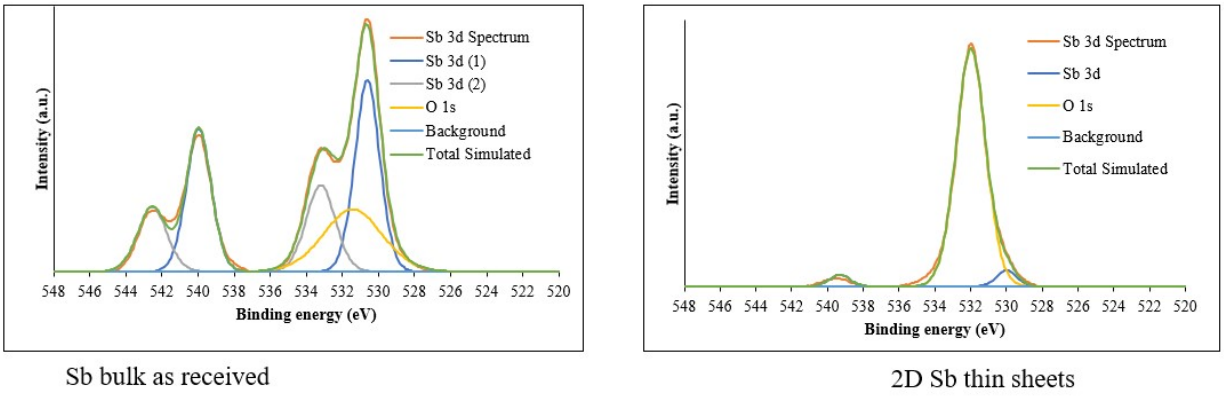

Figure S6. XPS spectra of Sb bulk and 2D antimonene sheets formed under optimal conditions in Fig. 1.

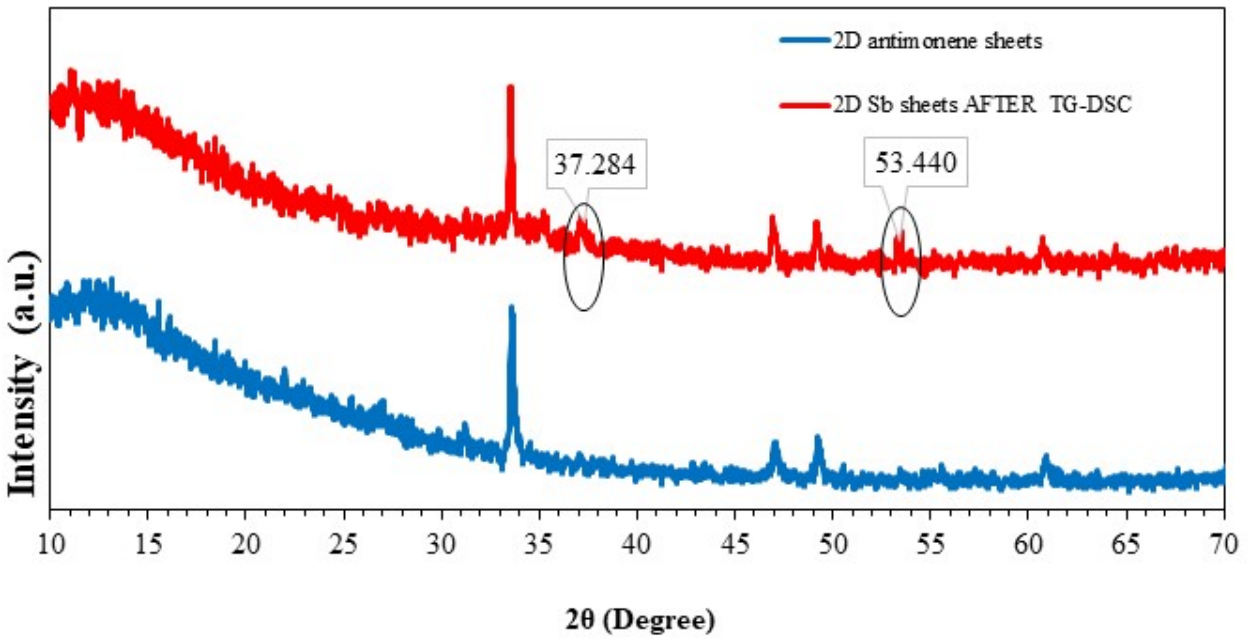

Figure S7. Co Kα XRD of 2D antimonene formed in VFD under optimal conditions and post-heating in TGA studies at 600 ° C.

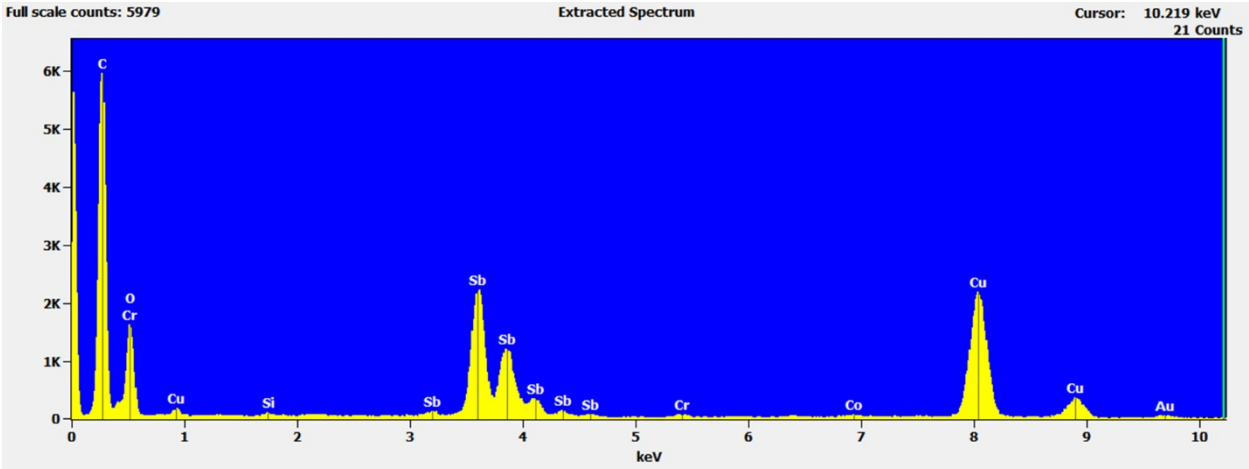

Figure S8. Sum spectra of TEM-EDX mapping of antimoene sheets on carbon-coated Cu grid that were synthesized using optimal conditions, Fig. 1.

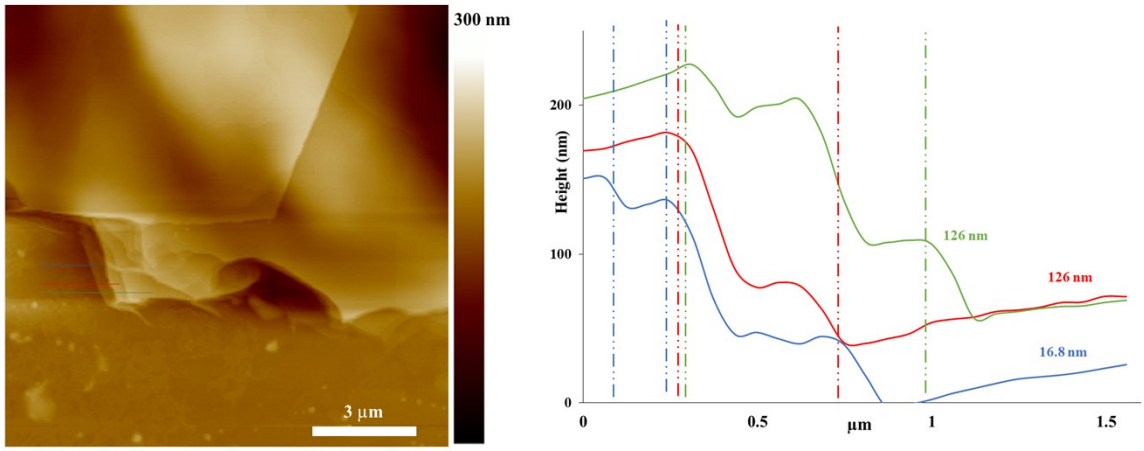

Figure S9. AFM image of antimonene sheets with thick 16.8- 126 nm synthesized in VFD in 2 min.

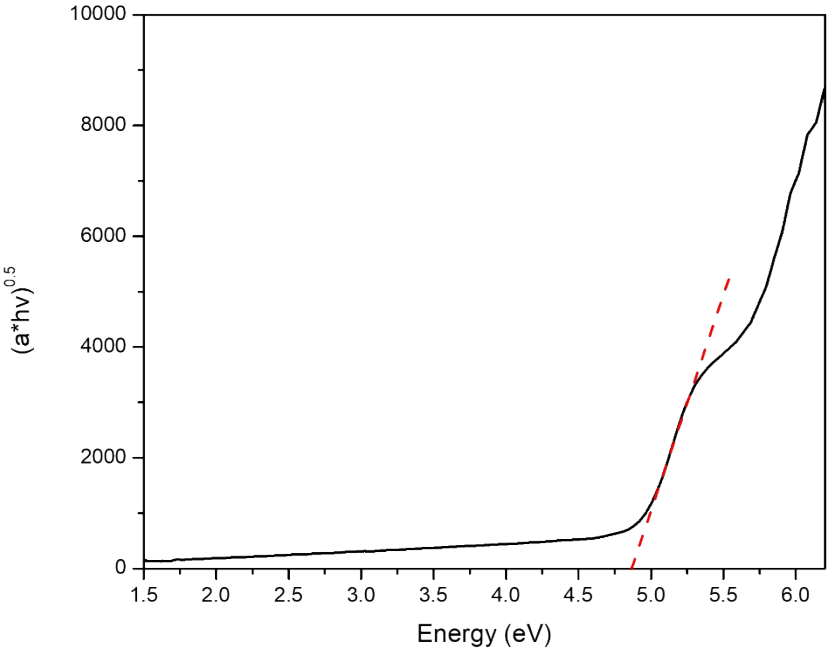

Figure S10. Tauc plot of antimonene sheets suspension for bandgap determine

Conducting AFM studies on 2D Sb sheets

Sb is an n-type dopant and along with phosphorous are the common n-type dopants of Si. When a metal forms a junction with an n-type semiconductor (M–S), the contact is rectifying (more conducting when the n-type Si is biased negative with respect to the metal) due to the formation of a Schottky barrier at the interface between metal (Pt) and semiconductor (Si). The Schottky barrier is formed due to misalignment between metal and semiconductor work functions. The barrier width (i.e. width of the depletion region) is controlled by the concentration of the dopants i.e. a smaller barrier width corresponds to higher doping.

In the case of moderately doped n-type Si, the Schottky barrier leads to the current being blocked when the Si surface is biased positive as shown in Figure. 4 (e). Increasing the Si doping is one of the common methods for decreasing the barrier width, which consequently enables current to pass when the Si is biased positive.

When present in high concentration, Sb doping decreases the barrier width at the metal/Si interface leading to the desired ohmic contact. In industry, Sb doping is usually added during the formation of the Si boule - a process that often gives each Si wafer a uniform doping. However, to define circuit elements especially at the nanoscale, processes such as diffusion and ion implantation dope selected areas— typically controlled by photolithography, with the latter method providing better control. It is therefore important to find methods to dope Si at specific locations on Si at the nanoscale. For instance, self-assembled molecular monolayer doping has been suggested for nanoscale doping.

Here, we show that the VFD fabricated 2D antimonene layers have the same effect as doping Si. When in contact with clean Si-H, the 2D antimonene layers induce switching from a rectifying to a non-rectifying ohmic contact Figure. (f-h) and SI Figure. S10 (a and b). This represents an important alternative to self-assembled molecular monolayer doping which involves dopant-containing molecular monolayers bonded onto hydrogen-terminated semiconductor surfaces.

Si–H surfaces preparation for current–voltage measurments

N-type (phosphorus doped) single-side polished Si wafer with the thickness ranging from 475-525 μm and (111) ± 0.05° (with resistivity of 0.01-0.1 Ω.cm) was used. Si wafers were first washed by

dichlooromethane (DCM), Isopropanol and Milli-Q water and then cleaned using piranha solution (3 H_2SO_4: 1 H_2O_2 (V/V)) at 130 °C for 30 min. The surface was subsequently etched in deoxygenated 40 wt % aqueous ammonium fluoride solution in the presence of small amount of ammonium sulfite monohydrate (~5 mg) for 13 min to remove the native oxygen layer on the Si surface and obtain H–terminated Si (Si–H). The etched surface was rinsed using Milli-Q water and DCM, and dried by nitrogen gas. Drop casting of Sb aqueous suspension was carried out on the surface of fresh Si–H.

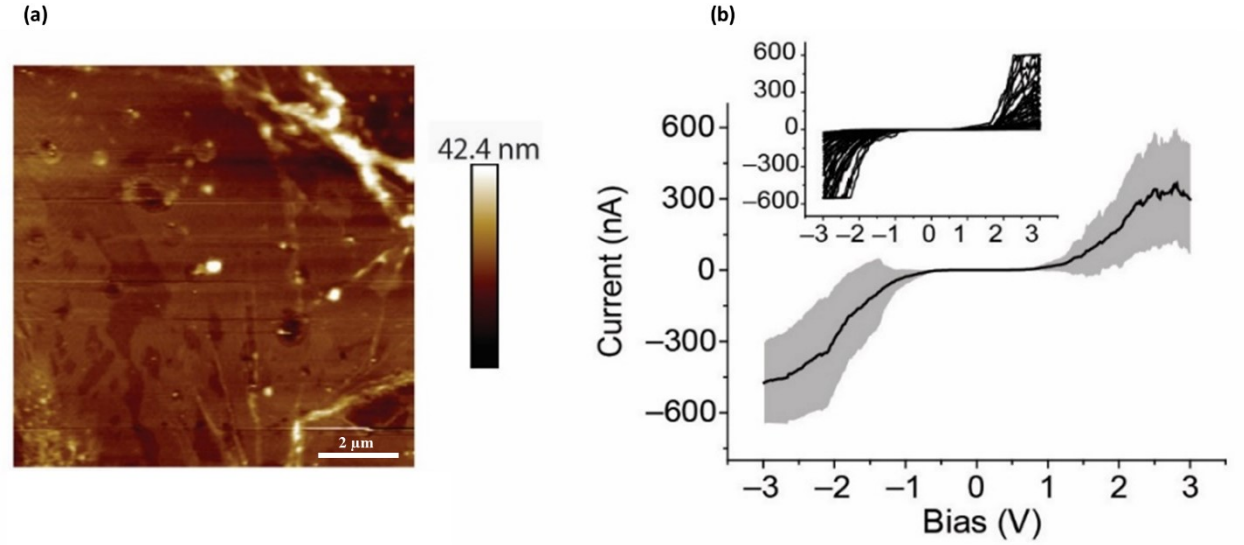

Figure S11. (a) AFM height topography of (Si−H)−Sb−Pt junction. (b) (I−V) measurements corresponding to the 2D-Sb sheet shown in (a). Inset in (b) demonstrates the overlay of 50 (I−V) curves measurements.

References:

1. J. Chen, X. Zhao, SJR Tan, H Xu, B Wu, B. Liu, d. Fu et al. "Chemical vapor deposition of large-size monolayer MoSe2 crystals on molten glass." *Journal of the American Chemical Society* 139, no. 3 (2017): 1073-1076.
2. X. Chen, Z. Zhang, B. Chen, C. Liu, S. Zhang, W. Cao, and Z. Wang, 2021. Crystalline grain refinement toughened isotactic polypropylene through rapid quenching of stretched melt. *Polymer*, 216, p.123435.
3. C. Gibaja, D. Rodriguez-San-Miguel, P. Ares, J. Gómez-Herrero, M. Varela, R. Gillen, J. Maultzsch, F. Hauke, A. Hirsch and G. Abellán, *Angewandte Chemie*, 2016, **128**, 14557-14561.
4. M. Assebban, C. Gibaja, M. Fickert, I. Torres, E. Weinreich, S. Wolff, R. Gillen, J. Maultzsch, M. Varela and S. T. J. Rong, *2D Materials*, 2020, **7**, 025039.
5. P. Ares, F. Aguilar-Galindo, D. Rodríguez-San-Miguel, D. A. Aldave, S. Díaz-Tendero, M. Alcamí, F. Martín, J. Gómez-Herrero and F. Zamora, *Advanced Materials*, 2016, **28**, 6332-6336.